Heteronuclear Cross-Relaxation Effects in the NMR Spectroscopy of Hyperpolarized Targets

Kevin J. Donovan, Adonis Lupulescu, and Lucio Frydman*[a]

Dissolution dynamic nuclear polarization (DNP) enables high-sensitivity solution-phase NMR experiments on long-lived nuclear spin species such as ^{15}N and ^{13}C. This report explores certain features arising in solution-state ^1H NMR upon polarizing low-γ nuclear species. Following solid-state hyperpolarization of both ^{13}C and ^1H, solution-phase ^1H NMR experiments on dissolved samples revealed transient effects, whereby peaks arising from protons bonded to the naturally occurring ^{13}C nuclei appeared larger than the typically dominant ^{12}C-bonded ^1H resonances. This enhancement of the satellite peaks was examined in detail with respect to a variety of mechanisms that could potentially explain this observation. Both two- and three-spin phenomena active in the solid state could lead to this kind of effect; still, experimental observations revealed that the enhancement originates from $^{13}C \rightarrow ^1H$ polarization-transfer processes active in the liquid state. Kinetic equations based on modified heteronuclear cross-relaxation models were examined, and found to well describe the distinct patterns of growth and decay shown by the ^{13}C-bound ^1H NMR satellite resonances. The dynamics of these novel cross-relaxation phenomena were determined, and their potential usefulness as tools for investigating hyperpolarized ensembles and for obtaining enhanced-sensitivity ^1H NMR traces was explored.

1. Introduction

Dissolution dynamic nuclear polarization (dDNP[1]) is a promising method to increase sensitivity in nuclear magnetic resonance (NMR) spectroscopy and imaging (MRI). Orders-of-magnitude enhancements can be delivered by dDNP for solution samples, depending on the targeted nucleus and on the kind of the observed system. Maximal post-dissolution enhancements are usually achieved by carrying out high-field cryogenic hyperpolarization on slowly relaxing nuclei, such as those arising in the non-protonated sites of small- or medium-sized molecules. For larger biomolecules and/or when targeting rapidly relaxing sites, such as ^1Hs, the cryogenic spin alignment is also high. However, the rapid relaxation experienced by the spins during the time elapsed between the sample dissolution and the high-resolution liquid-phase spectral acquisition, can rob the experiment from much of its usefulness. Several efforts have been proposed to surmount this problem, including storing magnetization as singlet states[2–5] and modifying the hardware to minimize the time during which the sample travels between the polarizing and the NMR fields.[6] Additional improvements in the sample-melting and injection procedures have recently enabled measuring dDNP NMR spectra of biomolecules.[7] Despite these advances, dDNP has been mostly confined to ^{13}C sites in small molecules with relatively long longitudinal relaxation times.[8–13]

A feature of the dDNP process rests in the fact that, prior to the dissolution and the transfer step, the sample is maintained at cryogenic conditions. Under these conditions the nuclear T_1s can become exceedingly long—minutes to hours—both for dilute and abundant nuclei. Given these long relaxation times the possibility arises to polarize multiple nuclei in a given sample, either by relying on simultaneous thermal mixing if electron linewidths are comparable to the nuclear Larmor frequencies,[14] or by targeting multiple DNP conditions if these profiles are characterized by resolved solid effects. In this latter instance one could first hyperpolarize the ^{13}C nuclei by irradiating the polarizing radical off-resonance by the ^{13}C Larmor frequency offset, and then switching the microwave pumping to protons by shifting the offset by the ^1H Larmor frequency. Given the relatively long cryogenic T_1 times of the ^{13}C (hours) in comparison to the ^1H DNP build-up times (minutes), no significant fraction of the previously created ^{13}C hyperpolarization would be lost. This study explores some of the features that arise when high-resolution liquid-state spectra are collected on a sample, in which the nuclei were polarized in this manner prior to the dissolution step. It was found that suitable hyperpolarization conditions can then lead to unusual liquid-state ^1H NMR spectra displaying intense peaks which result from the ^{13}C-bonded protons (satellite peaks). Furthermore, these conditions led to enhanced ^1H resonances persisting for times that exceeded the ^1H T_1 relaxation times of the targeted molecules in solution. A number of potential mechanisms, which could lead to such behavior, were examined. The leading cause was identified as cross-relaxation effects in solution. Potential ave-

[a] Dr. K. J. Donovan, Dr. A. Lupulescu, Prof. Dr. L. Frydman
Chemical Physics Department
Weizmann Institute of Science
Rehovot (Israel)
Fax: (+ 972) 8-934-4903
E-mail: lucio.frydman@weizmann.ac.il

nues for exploiting these effects to polarize rapidly relaxing nuclei such as [1]Hs in solutions, are put forward.

Materials and Methods

Dissolutions were performed using two different Oxford Instruments Hypersense® polarizers. NMR spectra were acquired using a 500 MHz Varian spectrometer and a 400 MHz Bruker spectrometer, on conventional 5 mm NMR double-resonance probes. Time-dependent post-dissolution ^{13}C and ^{1}H acquisitions were collected in a rapid and interleaved succession on the 500 MHz spectrometer; conventional 1D ^{1}H NMR series were collected at 400 MHz. BDPA (Sigma–Aldrich) was used as polarizing agent in all samples, at a 40 mM concentration. Pyridine and quinoline were mixed in equal proportions with $[D_6]DMSO$ to create their respective glassy matrices at low temperatures. Toluene was hyperpolarized undiluted as it self-glasses. All dissolutions were performed with approximately 4 mL methanol as the solvent, which rapidly melted and subsequently transferred the sample. Samples were polarized either at the full (≈ 180 mW) or half (≈ 100 mW) the power of the microwave unit. Simulations and fits were performed using Matlab® 7.10 (The Mathworks) and Mathematica (Wolfram). All spectra are displayed in reference to the transmitter offsets used for their respective acquisitions.

2. Results and Discussion

Figure 1 shows the basic phenomenon examined in this study, using pyridine as a prototypical organic dDNP target. Shown in Figure 1a is the conventional 1D ^{1}H NMR thermal spectrum. Dissolution counterparts arising upon preceding the NMR by DNP polarization at $-\omega_H$ and $+\omega_H$ offsets away from the central ω_e Larmor frequency of the polarizing radical are shown in Figure 1b and c. Given the relatively inefficient solid-effect process driving DNP for the B_0 field and for the radical used, the recording of opposite-phased resonances showing an approximately tenfold enhancement compared to the thermal counterpart, is as expected. Less intuitive are the 1D ^{1}H NMR spectra in Figure 1d and e, arising from acquisitions, in which the $\omega_e \pm \omega_H$ irradiation of the previous two experiments was preceded by approximately 3 h of microwave irradiation at the ^{13}C $\omega_e + \omega_c$ solid-effect conditions. Notice that in addition to the expected centerband behavior, these traces show the appearance of previously unobserved peaks with a phase-invariant behavior. The appearance of the new peaks in Figure 1d and e is not unique to pyridine. Figure 2 evidences their appearances in two additional simple compounds: toluene and quinoline. Although peak crowding in the 1D ^{1}H NMR spectrum of these compounds somewhat obscures the appearance of these new resonances, the difference between the traces arising after polarizing solely the ^{1}Hs versus those after subsequently polarizing the ^{13}C and the ^{1}H spins, is clear.

The central role played by ^{13}C in the generation of these unusual ^{1}H resonances is hinted at by the invariance of the latter with regards to the ^{13}C hyperpolarizing conditions (Figure 1). In addition, the role played by the ^{13}C can be observed in Figure 3, which illustrates the time progression of dDNP ^{1}H spectra acquired following the polarizations with $\omega_e + \omega_c$ (Figure 3b) and $\omega_e - \omega_H$ (Figure 3c). These small-tip-angle time
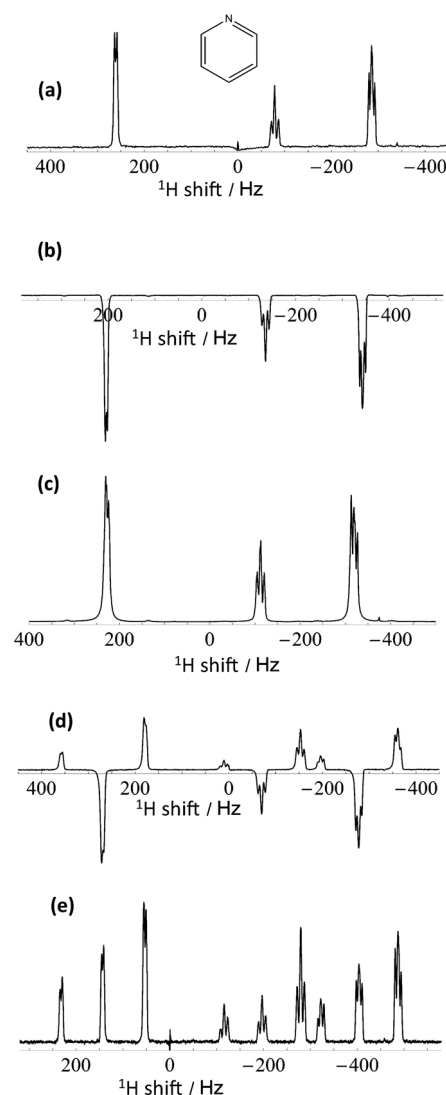

Figure 1. Single-scan 1D ^{1}H NMR spectra acquired on a) a pyridine sample at thermal equilibrium. b, c) Similar samples following hyperpolarization of the pyridine's ^{1}H nuclei for ≈ 20 min at $\approx \omega_e \pm \omega_H$, where ω denotes the Larmor frequency of the individual species. d, e) Idem, but after first hyperpolarizing the ^{13}C for ≈ 3 h at $\omega_e + \omega_c$, and then spending 20 min polarizing the ^{1}H nuclei as described in (b, c). See the Supporting Information for animated spectra of (d, movie 1) and (e, movie 2).

series, as well as more extensive ones, addressing pyridine and other compounds, are included in animated formats in the Supporting Information. All of these evidence an initial growth and subsequent decay of the anomalous peaks when pumping the ^{13}C DNP. In contrast, if only the ^{1}Hs are pumped, the ^{13}C-bound proton peaks mimic the mono-exponential decay of the ^{12}C-bound centerbands. Moreover, the anomalous peaks remain in their resonance positions as their intensities eventually decay into the usual appearance of ^{13}C-bound proton satellites, thereby confirming their origin.

The differences observed upon polarizing just the ^{1}Hs under cryogenic conditions versus the ^{1}H traces observed upon hyperpolarizing the heteronuclei suggest the onset of a multi-spin process that differentially affects ^{1}Hs bonded to ^{12}C and ^{13}C. Such processes are known to arise upon executing cryo-
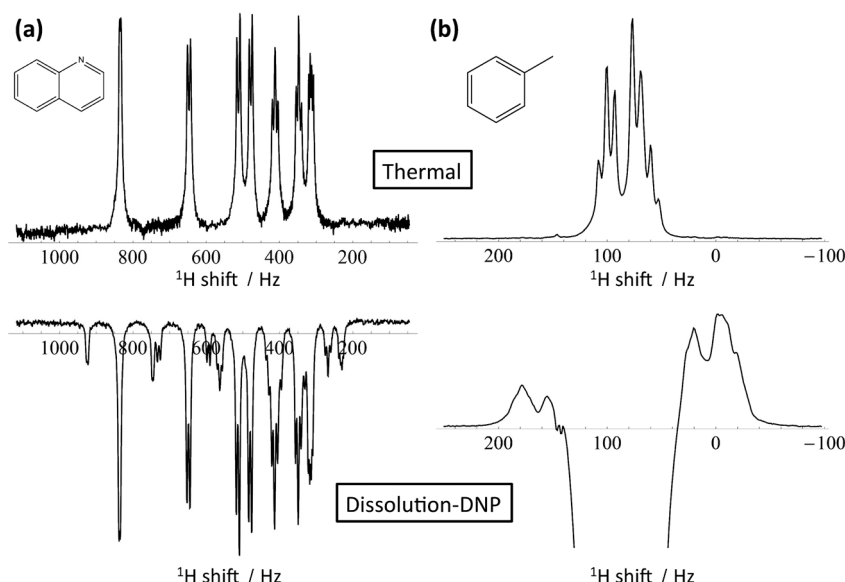
Figure 2. 1D ^{1}H NMR spectral from quinoline (a) and toluene (b) showing the appearance of anomalous peaks upon dDNP. Conventional spectra are shown at the top, acquired on the dissolution samples that were subject to dDNP after they have returned to thermal equilibrium. Shown at the bottom are hyperpolarized spectra acquired on these samples immediately after their dissolution and injection. In the quinoline hyperpolarized spectrum both the ^{12}C and the ^{13}C-bonded protons are polarized opposite to thermal polarization with the ^{13}C-bonded protons appearing disproportionately large at approximately half the intensity of the ^{12}C-bonded protons. Prior to injection the quinoline sample was polarized for 3 h at $\omega_e - \omega_C$, and then at $\approx \omega_e + \omega_H$ for 20 min. The toluene sample was prepared by polarizing for 3 h at $\omega_e + \omega_C$, and then at $\approx \omega_e + \omega_H$ for 20 min. See the Supporting Information for animated spectra of (a, movie 3) and (b, movie 4).
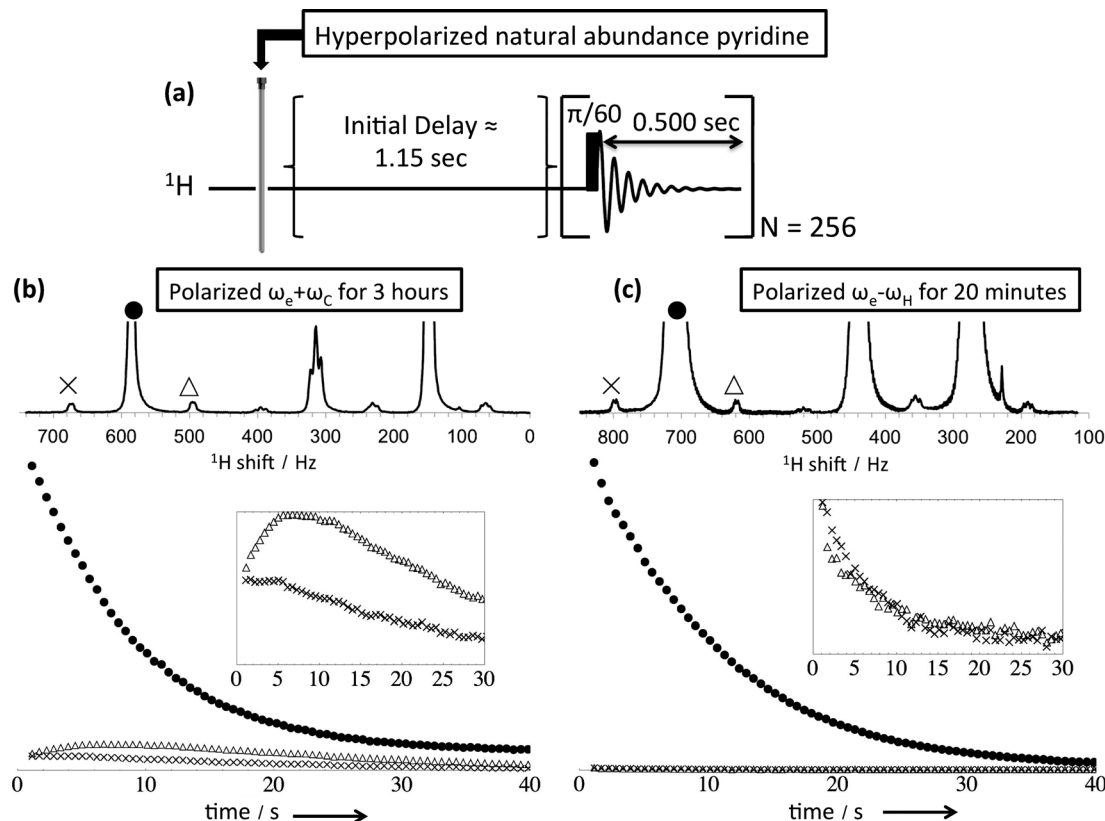
genic DNP experiments in the solid state;[14,15] it is further evidenced in the microwave frequency sweep shown in Figure 4, which reflects the ^{13}C polarization detected in the solid state for a pyruvic acid sample. Beyond the dominant double- and zero-quantum solid-effect peaks at $\omega_e \pm \omega_C$, minor resonant transfer phenomena are aligning the ^{13}C bulk magnetizations with opposite signs of polarization at microwave frequencies of $\omega_e \pm \omega_H \pm \omega_C/2$, that derive from simultaneous solid and cross effects.[16] A possible source of anomalous ^{1}H hyperpolarization could thus involve multiple forbidden transitions between all three spins—a double solid effect of the kind first described by de Boer.[17] To evaluate whether these effects could be relevant to the experiments in Figures 1 and 2, we consider an

Figure 3. a) Pulse sequence used to acquire the time progressions shown in (b) and (c). The top-most spectra illustrate initial ^{1}H NMR traces collected in these experiments right after sample injection; the bottom curves show the time evolution of the proton resonances marked by the crosses, solid dots, and triangles. Notice that anomalous peaks in (b) grow for approximately 8 s after injection; both the peak marked with x and the peak marked with (△) eventually decay into conventional ^{13}C satellites, reaching a steady value approximately one minute after injection. For the trajectory shown in (c) all proton resonances (both ^{12}C and ^{13}C-bonded) follow a similar mono-exponential decay to their equilibrium values.
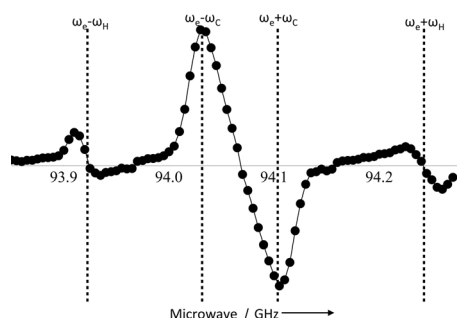
Figure 4. ^{13}C DNP enhancements observed in the solid state upon varying the microwave frequency. Dashed vertical lines indicate the (approximate) positions calculated for the microwave at frequencies $\omega_e \pm \omega_C$ and $\omega_e \pm \omega_H$, respectively. We ascribe the apparent non-linearity of these phenomena relative to the horizontal frequency axis, to the sweep's use of the microwave unit (Elva-1 VCOM-10) beyond its specified operating conditions. The frequency sweep was acquired on an Oxford Instrument Hypersense with approximately 100 µL of 40 mM BDPA in ^{13}C-enriched pyruvic acid. Each point in the microwave sweep was acquired following 10 min of microwave irradiation frequency at 177 mW power.

electron S coupled simultaneolusly to a ^{1}H and to a ^{13}C nucleus through hyperfine/dipole interactions and subjected to microwave irradiation. The relevant Hamiltonian is then [Eq. (1)]:

$$\mathscr{H} = \underbrace{\omega_{2S}S_z + \omega_H H_z + \omega_C C_z}_{\mathscr{H}_Z} + \underbrace{A_{z+}^{SH} S_z H_+ + A_{z+}^{SC} S_z C_+ + \cdots}_{\mathscr{H}_{HF}}$$
$$+ \underbrace{\omega_{MW} \cos(\omega t) S_x}_{\mathscr{H}_{MW}} \tag{1}$$

where $\mathscr{H}_Z$ describes the Zeeman coupling to the external magnetic field, $\mathscr{H}_{HF}$ accounts for the hyperfine/dipole interactions A, and $\mathscr{H}_{MW}$ represents the coupling to the oscillating field acting during the DNP process. The hyperfine interaction imparts small corrections to the Zeeman eigenstates; a detailed analysis shows that if the electron has significant hyperfine couplings to both ^{1}H and ^{13}C nuclei, second-order corrections to the Zeeman eigenstates may enable microwave-driven transitions between energy levels that are separated by $\omega_e \pm \omega_H \pm \omega_C$. Such transitions may in principle lead to enhanced polarization transfers to ^{1}H nuclei that are in close proximity to ^{13}Cs. However, since these three-spin phenomena are made possible by second-order corrections to the energy eigenstates, their associated transition rates must be significantly smaller than the rates responsible for the normal solid-effect process. A simple estimation of the ratio between the first-order transition rates enabling the two-spin solid effect and the second-order rates enabling these three-spin phenomena is given by Equation (2):

$$\left(\frac{\omega_{MW} A_{z+}^{SH}}{\omega_H}\right)^2 \bigg/ \left(\frac{\omega_{MW} A_{z+}^{SH} A_{z+}^{SC}}{\omega_H \omega_C}\right)^2 = \left(\frac{\omega_C}{A_{z+}^{SC}}\right)^2 \cong 1000 \tag{2}$$

with $\omega_C/2\pi = 35$ MHz and $A_{z+}^{SH,SC}/2\pi \cong 1$ MHz taken as typical values. Such ratio between the rates appears, however, too

small to lead to the significant ^{1}H enhancements in Figure 1 and 2, which exceed the conventional solid DNP effects of the ^{1}H centerbands by two orders of magnitude. Likewise, the emergence of hybrid solid/cross effects among the three spins by irradiation at $\omega_e \pm \omega_H \pm \omega_C/2$ would fail, by themselves, to account for the entirety of these phenomena.

Another phenomenon that could be relevant in these multinuclear DNP effects, rests on the truncated ^{1}H–^{1}H spin diffusion, which arises upon replacing a ^{12}C with a ^{13}C nucleus. The dipolar coupling between bonded ^{13}C and ^{1}H spins could truncate ^{1}H–^{1}H spin-diffusion effects, and by doing so enrich the polarization of the ^{13}C-bonded sites. In an effort to explore this effect a number of simulations were performed on multiple-spin ^{13}C-^{1}H-(^{1}H)$_4$ systems with active nuclear dipole–dipole couplings and compared against counterparts which lacked the ^{13}C species. In such calculations the initial source of polarization was presumed to be at the carbon-bonded proton and its transfer of polarization to the remaining bulk was examined. The plots illustrated in Figure 5, suggest that an additional ^{13}C-dipolar coupling may indeed lead to an enhanced polarization of the directly bonded proton. This phenomenon alone, however, cannot explain the multi-fold enhancement of the spectral ^{1}H satellite patterns observed in the liquid state.

It follows from these arguments that while unusual multi-spin processes may occur during cryogenic hyperpolarization, the relative contributions of these mechanisms cannot by themselves explain the results in Figures 1 and 2. With this as premise we focused on heteronuclear cross-relaxation processes happening once the sample has been melted and transferred into high fields as the main cause of the anomalous ^{1}H peaks. Such processes have been noted by Merritt et al. in ^{13}C-labeled formate samples.[18] To describe the behavior of protons under the influence of heteronuclear cross-relaxation effects in our ^{13}C-hyperpolarized samples we went beyond the
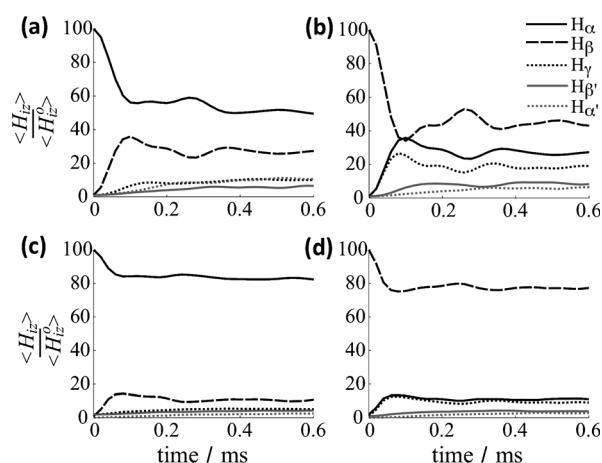

Figure 5. Simulated time evolution of the proton polarization in solid pyridine starting from a non-equilibrium initial state. a) ^{1}H polarization dynamics with all carbon sites occupied by the ^{12}C isotope and the H$_\alpha$ proton being initially hyperpolarized. b) As in (a) except that the H$_\beta$ proton is initially hyperpolarized. c) Polarization dynamics starting from the same initial state as in (a) but with C$_\alpha$ site occupied by the ^{13}C isotope. d) Polarization dynamics starting from the same initial state as in (b) but with C$_\beta$ site occupied by a ^{13}C isotope.

basic Solomon analysis used in that study,[19] and refer instead to Goldman's description[20] of a two-spin heteronuclear system in liquids, modified to account for the presence of large chemical shift anisotropies (CSAs) on both the ^{1}H and ^{13}C spins involved. Using a notation analogous to Goldman's, the relevant Equations (3a–c) are then:

$$\frac{dH_z}{dt} = -\left(A_1 - \frac{1}{T_1^H}\right)(H_z - 2H_0) - E_1(C_z - 2C_0) - \mathbf{B}_1 \cdot 2H_zC_z \tag{3a}$$

$$\frac{dC_z}{dt} = -A_1'(C_z - 2C_0) - E_1(H_z - 2H_0) - \mathbf{B}_1' \cdot 2H_zC_z \tag{3b}$$

$$\frac{d2H_zC_z}{dt} = -\mathbf{B}_1(H_z - 2H_0) - \mathbf{B}_1'(C_z - 2C_0) - \left(C_1 + \frac{1}{T_1^C}\right) \cdot 2H_zC_z \tag{3c}$$

Parameters involved in these equations include [Eqs. (4a–i)]:

$$A_1 = D\tau_c\left\{\frac{6(1+\alpha_H^2)}{1+\omega_H^2\tau_c^2} + \frac{2}{1+(\omega_H-\omega_C)^2\tau_c^2} + \frac{12}{1+(\omega_H+\omega_C)^2\tau_c^2}\right\} \tag{4a}$$

$$A_1' = D\tau_c\left\{\frac{6(1+\alpha_C^2)}{1+\omega_C^2\tau_c^2} + \frac{2}{1+(\omega_H-\omega_C)^2\tau_c^2} + \frac{12}{1+(\omega_H+\omega_C)^2\tau_c^2}\right\} \tag{4b}$$

$$B_1 = D\tau_c\left\{\frac{12\alpha_H}{1+\omega_H^2\tau_c^2}\right\} \tag{4c}$$

$$B_1' = D\tau_c\left\{\frac{12\alpha_C}{1+\omega_C^2\tau_c^2}\right\} \tag{4d}$$

$$C_1 = D\tau_c\left\{\frac{6(1+\alpha_H^2)}{1+\omega_H^2\tau_c^2} + \frac{6(1+\alpha_C^2)}{1+\omega_C^2\tau_c^2}\right\} \tag{4e}$$

$$E_1 = D\tau_c\left\{\frac{2}{1+(\omega_H-\omega_C)^2\tau_c^2} + \frac{2}{1+(\omega_H-\omega_C)^2\tau_c^2}\right\} \tag{4f}$$

$$D = \frac{1}{20}\gamma_H^2\gamma_C^2\hbar^2 r^{-6} \tag{4g}$$

$$\alpha_H = \frac{2}{3}B_0(\sigma_{\parallel,H} - \sigma_{\perp,H})r^3/(\gamma_H\hbar) \tag{4h}$$

$$\alpha_C = \frac{2}{3}B_0(\sigma_{\parallel,C} - \sigma_{\perp,C})r^3/(\gamma_C\hbar) \tag{4i}$$

where τ_c is the correlation time, r is the internuclear distance between a proton and its directly bonded ^{13}C, α_H and α_C give the ratios of CSA to the heteronuclear dipolar fields for each species, $\sigma_\parallel$ and $\sigma_\perp$ are the respective components (parallel and perpendicular) of the assumed-axial CSA tensors of the two sites in their principal axes systems, T_1^H and T_1^C are phenomenological longitudinal proton and carbon relaxation times unrelated to the specific ^{13}C–^{1}H pair (e.g. T_1^H would take into account mechanisms that control relaxation of the ^{12}C-bonded ^{1}Hs), and $\hbar$ is the reduced Planck constant. Taking the ^{13}C-bonded protons as a doublet spin system, the individual resonances appearing in their spectrum are given by Equations (5a) and (5b):

$$H_z^{(1)} = (H_z - 2H_zC_z)/2 \tag{5a}$$

$$H_z^{(2)} = (H_z + 2H_zC_z)/2 \tag{5b}$$

With this formalism at hand, we set out to fit the data observed in the dissolution trajectories of pyridine and explore if solution cross-relaxation effects could by themselves give a qualitative and quantitative understanding of the anomalous ^{1}H spectra. (A precaution taken in the fitting of these data included a correction to account for magnetization losses due to pulsing.[21–22]) Figure 6 shows two examples of dissolution ^{1}H and ^{13}C NMR experiments, corresponding to different initial conditions of the ^{13}C hyperpolarization. Simulations show a close fit to the acquired data upon adopting $\Delta\sigma_C = |\sigma_{\parallel,C} - \sigma_{\perp,C}| = 120$ ppm for the ^{13}C and $\Delta\sigma_H = 10$ ppm for the bonded ^{1}Hs, an internuclear distance of $r = 1.08$ Å, and a non-^{13}C-derived ^{1}H relaxation loss of $T_1^H = 13.4$ and 11.7 s for Figure 6a and b (akin to the T_1 measured by a conventional inversion recovery sequence[23] for the ^{12}C-bonded ^{1}Hs: $T_1 \approx 6.75$ s at 400 MHz). The initial ^{13}C polarization at the time at which the sample was injected into the NMR tube was also fitted, giving a best match when set to approximately 14 000 and -8 000 times their thermal counterpart, consistent with other enhancements achieved when using dDNP hardware and methods. Fitting the post-dissolution data also required a τ_c; Figure 6 leads to correlation times of 2.75 ± 0.25 ps, a reasonable fit to the $\tau_c = 1.85$ ps value previously measured for pure pyridine at a slightly different temperature.[24]

The good fit between this model and the experimental time series confirms that the extent of the ^{13}C hyperpolarization directly bears on the extent to which ^{13}C-bonded protons increase their satellites' intensities. During their initial growth period these post-dissolution fits indicate that the hyperpolarized ^{13}C nuclei transfer approximately 10% of their initial polarizations to the bonded protons, reaching a maximum after about 10 s. The ^{1}H enhancement then persists for approximately a time period of five times T_1^C, and the higher the degree of ^{13}C hyperpolarization is, the stronger are the satellites in the corresponding ^{1}H NMR spectrum. Furthermore, the direction in which these proton satellite transitions grow relative to the ^{1}H centerband is determined by the direction of ^{13}C polarization (Figure 6).

A feature evidenced by all experiments is the systematic difference in the initial intensities of the proton satellites. Analysis of the formalisms embodied by Equations (3)–(5), however, predicts that in the initial absence of the bilinear spin term $2H_zC_z$, the intensities of the ^{1}H satellites should have identical intensities. Only the onset of different cross-relaxation effects acting on each $H_z^{(1,2)}$ component of this doublet, due to the combined dipolar/CSA effects, should eventually endow these peaks with a growing asymmetry. This point raises again the possibility that some anomalous phenomenon is already active at time zero; that is, some form of two-spin order originates already in the solid phase or over the course of the low-field sample transfer.[25] However, sample settling in dDNP is a process requiring a certain time before the NMR observations can be carried out; an interval over which the relaxation effects
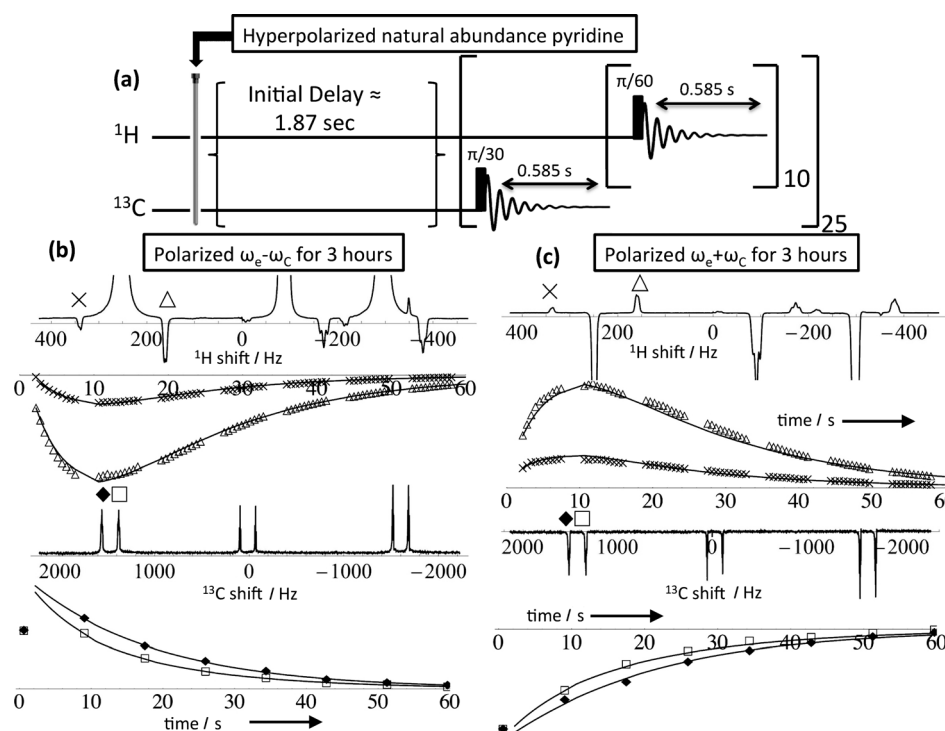
Figure 6. a) Pulse sequence used for fitting the relaxation-driven time progress of ^1H satellite peaks, based on fitting alternating proton and ^{13}C acquisitions on the same hyperpolarized samples. b,c) Fits for the time-dependent evolution of the indicated pyridine ^1H and ^{13}C NMR peaks when the sample was polarized at $\omega_e - \omega_C$ (left) and $\omega_e + \omega_C$ (right) for 3 h. These fits were calculated by successive iteration of Equations (3a–3c) and are shown in all plots as solid black lines. Additional details are given in the main text.
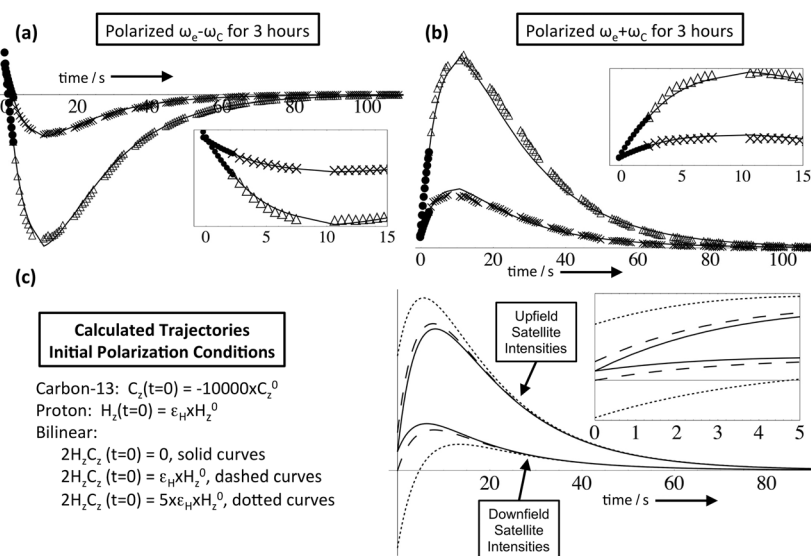

Figure 7. a, b) Back-extrapolation of the time-dependent ^1H satellite evolutions introduced in Figure 6, with black dots indicating data that were calculated on the basis of Equations (3–5) from the first experimental data point, back to the approximate time of injection. Plot insets show that at an estimated time of sample injection of 2.2 s, the back-calculated satellite intensities are nearly equal. c) Simulations of the ^{13}C ^1H satellites' evolution in dDNP experiments, in which the heteronuclear polarization transfer is governed by Equations (3–5), but in which different extents of the bilinear spin term $2H_zC_z$ were assumed to be present at the time of injection. These calculations also assumed a $-10000x$ ^{13}C hyperpolarization (relative to its thermal equilibrium at 11.74 T), and a ^1H nuclear enhancement of $\varepsilon_H \approx 57$ (which is the enhancement expected from transferring an equilibrated sample from 1.5 K and 3.35 T, into a 298 K and 11.74 T NMR setting). Simulations were conducted for three initial amounts of bilinear spin order, revealing an increasing difference between the magnetizations of the two ^{13}C-bonded proton transitions and increasing deviations from the experimental observations. These results suggest minimal contributions, if any at all, of $2H_zC_z$ bilinear spin order arriving from the solid phase.

summarized in Equations (3)–(5) could already have been active. Given that data of the kind illustrated in Figure 6 yields an accurate fit of the parameters involved in the cross relaxation. These fitting parameters could be used to back-calculate the nature of the heteronuclear polarization transfer present at the approximate time of injection, which is a blind spot in the dDNP methodology. It is in the order of 2 s, yet it is not 100% reproducible and hence not known with perfect precision. This uncertainty notwithstanding, Figure 7 presents an estimate of what the polarizations of the individual proton satellites could have been when the sample was injected into the NMR tube at the high magnetic field. Looking at the results of these back-calculations of the dissolution trajectories, it follows that there is most likely a minimal amount of the bilinear spin term $2H_zC_z$ in the system at the time of injection. The back-extrapolations indicate that the two transitions of the ^{13}C-bound proton doublet have approximately the same magnitude of about 2.2 s before the first spectral acquisition, which is a reasonable time for these methanol-driven sample injections. The sample-settling conditions were optimized with a chase-gas time of 1.75 s and a settling time of approximately 0.12 s, followed immediately by a first spectral acquisition collected on the ^{13}C nuclei.

A final feature worth remarking is that the cross-correlated relaxation model always predicts that one of the components in the ^1H satellite doublet (the one associated with the $\left| -\frac{1}{2} \right\rangle$ ^{13}C eigenstate) reaches the highest absolute polarization. This occurs regardless of the absolute direction of the ^{13}C polarization. The spectral sets illustrated in Figure 8 demonstrate a way of
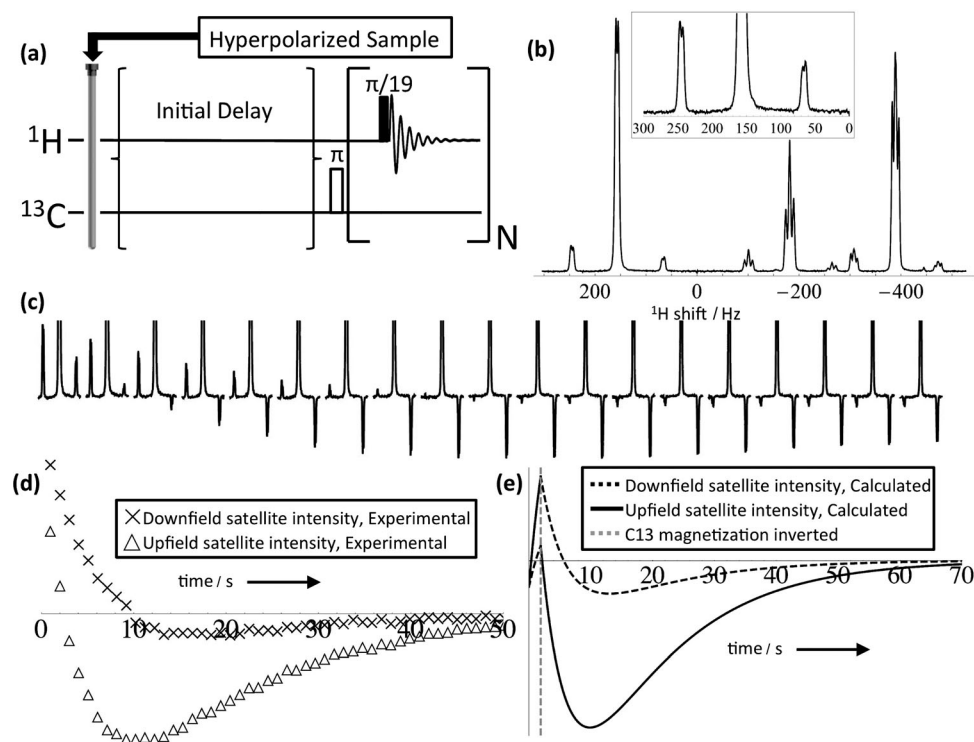
Figure 8. Manipulating the modulation of the ^{1}H satellites by ^{13}C-based pulses. a) A pyridine sample was initially polarized at $\omega_e + \omega_C$ for 2 h, then at $\approx \omega_e + \omega_H$ for 20 min, followed by the pulse sequence shown. This included an initial delay of ≈ 2 s, a hard 180° ^{13}C pulse, and the collection of a series of ^{1}H spectra in succession with small flip-angle pulses. b) First ^{1}H spectrum in the series, emphasizing an asymmetry in the ^{13}C-bonded satellites which is opposite to the asymmetries shown in all previous spectra of this study. c) Complete time series evolved by the upfield H$_\alpha$ resonance, with acquisitions being approximately 1 s apart revealing the unusual evolution of the individual satellite transitions before gradually returning to their equilibrium values. d,e) Summary of the experimental satellite peak intensities and expectations from Equations (3–5), with the dashed line indicating the time at which the hyperpolarized ^{13}C magnetization was inverted. See the Supporting Information for the animated spectrum of (b, movie 5).

reversing/controlling this condition. The corresponding experiments involve inversion of the ^{13}C populations immediately after sample injection, and allowance of ^{13}C→^{1}H transfer by cross relaxation; notice that proton doublets then end up with an opposite asymmetry than in all the other spectra shown in this report. The overall intensity of the individual proton satellites also undergoes a peculiar trajectory, crossing the zero-intensity line a number of times over the course of their evolution. Calculations based on Equations (3)–(5) are consistent with this train of events, predicting that when the ^{13}C population is inverted the relative intensities of the ^{1}H satellites will also be reversed (as a result of the 180° pulse inverting the bilinear magnetization term $2H_zC_z$) and so will the direction of their polarization's enhancement by reaching a maximum and eventually decaying to the thermal equilibrium values (Figure 8 e). This manipulation illustrates how modulations in the sense of the ^{13}C polarization are directly mapped into the signals arising from its bonded satellites. This, in combination with the long lifetimes supported by the ^{13}C spins, opens new ways for the acquisition of 2D heteronuclear correlations in systems subject to this kind of hyperpolarization.

4. Conclusions

This study discussed aspects arising in ^{1}H solution-phase NMR when dealing with a combination of strongly non-thermal ^{13}C polarizations, sizable ^{13}C relaxation times, and cross-relaxation effects. All these factors can lead to a significant and selective enhancement of the ^{1}H satellite signals driven by the ^{13}C hyperpolarization. This was demonstrated by sequentially hyperpolarizing carbon and/or protons and observing the ensuing ^{1}H NMR spectra in natural-abundance samples; similar effects should arise in systems including enriched ^{13}C materials, or other DNP target nuclei such as ^{15}N. The resulting enhancements could be further leveraged by collapsing the heteronuclear J-multiplets into single-site resonances applying decoupling or other strategies,[26] which this study did not attempt, in order to better illustrate the new physical phenomena being targeted. The time-dependent ^{1}H polarization gains could be well explained by established models for heteronuclear polarization transfer with realistic and convincing values. Although contemplated, no evidence was found regarding the presence of anomalous pre-dissolution solid-state DNP effects such as spin-diffusion quenching or three-spin processes; neither was there evidence for the formation in the solid or over the course of the low-field transfer process of multi-spin-ordered states.

The ensuing experiments spontaneously achieved high ^{1}H polarizations and preserved them on timescales given largely by the T_1^C, which was close to a minute in the present study. It is interesting to compare these spontaneous polarization transfer processes with analogs based on J-transfers that are discussed in the hyperpolarized literature.[8, 10-13, 27-30] Although it is likely that coherent transfer sequences such as INEPT could lead to larger single-shot ^{1}H signals, the mechanism presented here evidences a number of advantageous features. These include a simplicity that would be welcome in single resonance systems (including MRI scanners) and a predictable and long-lived nature of the transfer that enables the simple acquisition of arrays of ^{1}H-enhanced spectra. This could, in turn, prove valuable for achieving further enhancements in 1D ^{1}H NMR acquisitions than what was here described, as well as ^{1}H-based 2D NMR acquisitions. This phenomenon could also have potential in heteronuclear correlations, for which one seeks to

select only coupled spin systems while suppressing ^{12}C-bonded protons; a topic of significant recent interest.[31–33] These and other potential uses are currently under investigation.

Acknowledgements

[1] J. H. Ardenkjær-Larsen, B. Fridlund, A. Gram, G. Hansson, L. Hansson, M. H. Lerche, R. Servin, M. Thaning, K. Golman, *Proc. Natl. Acad. Sci. USA* **2003**, *100*, 10158 – 10163.

[2] A. Carravetta, O. G. Johannessen, M. H. Levitt, *Phys. Rev. Lett.* **2004**, *92*, 153003 – 153007.

[3] A. Carravetta, M. H. Levitt, *J. Am. Chem. Soc.* **2004**, *126*, 6228 – 6229.

[4] W. S. Warren, E. Jenista, R. T. Branca, X. Chen, *Science* **2009**, *323*, 1711 – 1714.

[5] P. R. Vasos, A. Comment, R. Sarkar, P. Ahuja, S. Jannin, J. P. Ansermet, J. A. Konter, P. Hautle, B. van der Brandt, G. Bodenhausen, *Proc. Natl. Acad. Sci. USA* **2009**, *106*, 18469 – 18473.

[6] J. Leggett, R. Hunter, J. Granwehr, R. Panek, A. J. Perez-Linde, A. J. Horsewill, J. McMaster, G. Smith, W. Kockenberger, *Phys. Chem. Chem. Phys.* **2010**, *12*, 5883 – 5892.

[7] S. Bowen, C. Hilty, *Phys. Chem. Chem. Phys.* **2010**, *12*, 5766 – 5770.

[8] L. Frydman, D. Blazina, *Nat. Phys.* **2007**, *3*, 415 – 419.

[9] M. G. Saunders, C. Ludwig, U. L. Gunther, *J. Am. Chem. Soc.* **2008**, *130*, 6914 – 6915.

[10] S. Bowen, H. Zeng, C. Hilty, *Anal. Chem.* **2008**, *80*, 5794 – 5798.

[11] M. Mishkovsky, L. Frydman, *ChemPhysChem* **2008**, *9*, 2340 – 2348.

[12] P. Giraudeau, Y. Shrot, L. Frydman, *J. Am. Chem. Soc.* **2009**, *131*, 13902 – 13903.

[13] H. Zeng, Y. Lee, C. Hilty, *Anal. Chem.* **2010**, *82*, 8897 – 8902.

[14] W. de Boer, M. Borghini, K. Morimoto, T. O. Niinikoski, F. Udo, *J. Low Temp. Phys.* **1974**, *15*, 249 – 267.

[15] M. Borghini, W. de Boer, K. Morimoto, *Phys. Lett. A* **1974**, *48*, 244 – 246.

[16] S. Reynolds, H. Patel, *Appl. Magn. Reson.* **2008**, *34*, 495 – 508.

[17] W. de Boer, *J. Low Temp. Phys.* **1976**, *22*, 185 – 212.

[18] M. E. Merritt, C. Harrison, W. Mander, C. R. Malloy, A. D. Sherry, *J. Magn. Reson.* **2007**, *189*, 280 – 285.

[19] I. Solomon, *Phys. Rev.* **1955**, *99*, 559 – 565.

[20] M. Goldman, *J. Magn. Reson.* **1984**, *60*, 437 – 452.

[21] A. W. Barb, S. W. Hekmatyar, J. N. Glushka, J. H. Prestegard, *J. Magn. Reson.* **2011**, *212*, 304 – 310.

[22] B. R. Patyal, J. H. Gao, R. F. Williams, J. Roby, B. Saam, B. A. Rockwell, R. J. Thomas, D. J. Stolarski, P. T. Fox, *J. Magn. Reson.* **1997**, *126*, 58 – 65.

[23] R. L. Vold, J. S. Waugh, M. P. Klein, D. E. Phelps, *J. Chem. Phys.* **1968**, *48*, 3831 – 3832.

[24] D. Schweitzer, H. W. Spiess, *J. Magn. Reson.* **1974**, *15*, 529 – 539.

[25] M. C. D. Tayler, I. Marco-Rius, M. I. Kettunen, K. M. Brindle, M. H. Levitt, G. Pileio, *J. Am. Chem. Soc.* **2012**, *134*, 7668 – 7671.

[26] P. Andersson, J. Weigelt, G. Otting, *J. Biomol. NMR* **1998**, *12*, 435 – 441.

[27] M. Mishkovsky, L. Frydman, *Ann. Rev. Phys. Chem.* **2009**, *60*, 429 – 448.

[28] C. Ludwig, I. Marin-Montesinos, M. G. Saunders, U. L. Gunther, *J. Am. Chem. Soc.* **2010**, *132*, 2508 – 2509.

[29] T. Harris, P. Giraudeau, L. Frydman, *Chem. Eur. J.* **2011**, *17*, 697 – 703.

[30] K. J. Donovan, L. Frydman, *J. Magn. Reson.* **2012**, *225*, 115 – 119.

[31] J. R. Garbow, D. P. Weitekamp, A. Pines, *Chem. Phys. Lett.* **1982**, *93*, 504 – 509.

[32] C. Emetarom, T. L. Hwang, G. Mackin, A. J. Shaka, *J. Magn. Reson.* **1995**, *115*, 137 – 140.

[33] A. Lupulescu, G. L. Olsen, L. Frydman, *J. Magn. Reson.* **2012**, *218*, 141 – 146.